

PSFC/JA-04-31

**DIVIMP modeling of impurity flows and screening in Alcator
C-Mod**

T. Chung*, I.H. Hutchinson, B. Lipschultz, B. LaBombard, S.
Lisgo[†]

14 September 2004

Plasma Science and Fusion Center
Massachusetts Institute of Technology
Cambridge, MA 02139 USA

[†]UTIAS
University of Toronto
Toronto, Ontario, Canada

This work was supported by the U.S. Department of Energy, Cooperative Grant No. DE-FC02-99ER54512. Reproduction, translation, publication, use and disposal, in whole or in part, by or for the United States government is permitted.

DIVIMP modeling of impurity flows and screening in Alcator C-Mod

T. Chung^{*}, I. H. Hutchinson, B. Lipschultz, B. LaBombard, S. Lisgo^a

M.I.T. Plasma Science and Fusion Center, Cambridge, MA 02139 USA

^a *UTIAS, University of Toronto, Toronto, Ontario, Canada*

Abstract

We report on impurity transport modeling using the DIVIMP code which is able to qualitatively reproduce the poloidal variation of non-recycling impurity penetration factor (PF_{NR}) found in C-Mod experiments: a lower PF_{NR} is computed at the inboard (3.6 %) and divertor target locations (0.7 %) than at the outboard (11 %). By artificially increasing the modeled inner SOL plasma flow to correspond to measured values, a better quantitative agreement between modeled and measured PFs is achieved. We have also roughly reproduced the observed penetration factor for recycling impurities both in time dependence and magnitude. The model has shown that under attached conditions, the majority of recycling impurity ions flow into the confined plasma through the outboard side separatrix. For detached conditions the impurity influx across the separatrix is more concentrated near the divertor.

PACS: 52.55.F, 52.65.K, 52.25.V

JNM keywords: Impurities (I0100), Plasma-Materials Interaction (P0500)

PSI-16 keywords: Alcator C-Mod, DIVIMP, Recycling, Impurity screening

**Corresponding author address:* 175 Albany St. NW17-103, Cambridge, MA 02139, USA

**Corresponding author E-mail:* blip@psfc.mit.edu

**Corresponding Author Phone/FAX:* 1-617-253-8636, 1-617-253-0627

**Corresponding Author:* Bruce Lipschultz

1. Introduction

Impurity screening studies in C-Mod have shown that the screening of non-recycling impurities, defined as a ‘penetration factor (PF_{NR})’, injected at the inboard edge is higher than impurities injected from the outboard by a factor of 20 or more [1]. The PF_{NR} for divertor originating impurities was midway between that of the outer and inner midplanes. Recycling impurities were found to have a penetration factor, PF_R that was independent of launch location [2]. Although qualitative interpretation of impurity screening has been proposed in the experiments, the underlying physics are not yet clear. We explore the underlying physics in this study using the DIVIMP code [3]. Three Ohmic L-modes plasmas are modeled with line averaged densities 1.1, 1.46, and $2.1 \times 10^{20} \text{ m}^{-3}$. For the highest density plasma the outer divertor is detached.

2. DIVIMP Modeling

DIVIMP [3] is an impurity transport code based on Monte-Carlo techniques. For the present study, the code has been modified to include additional physical effects and provide extra diagnostic information [4]. Fig.1 shows the DIVIMP grid which indicates the various locations for impurity recyclings which were added; the inner wall surfaces via radial diffusion (IWL), on discrete locations of the outboard vessel via parallel transport along field-lines outside the grid (PL1, PL2, PL3, and PL4), and on the antenna limiter via perpendicular diffusion (OWL). In this figure, the grid edge index for where the impurity neutral entered the grid, and the separatrix index (circled number) for characterizing the impurity influx across the separatrix, are indicated. Impurities recycled on the divertor are re-injected with a cosine angular distribution and specified fraction of injection energy dependent on energy and particle reflection coefficients [5]. We have

also implemented a method of measuring the impurity influx penetrating into the core (confined plasma) across the separatrix by what we call the **sepxing** counter. **Sepxing** keeps track of the origin of a core penetrating ion, i.e. it notes which solid surface the particle last touched before crossing the separatrix. A constant impurity diffusion coefficient of $0.1 \text{ m}^2/\text{sec}$ is used everywhere on the grid.

The background plasma is prescribed on the computational grid (Fig.1). For the description of the SOL plasma, a simple 1-D onion-skin model (OSM) [6] is employed. The electron parallel heat conduction in the parallel direction (ds) is solved to obtain the plasma temperature (assuming $T_e = T_i$),

$$q_e = -\kappa_e T_e^{2.5} \frac{dT_e}{ds} (\text{W} / \text{m}^2) \quad (1)$$

where κ_e is the electron thermal conductivity ($\sim 2,000 \text{ W eV}^{-3.5}/\text{m}$), T_e is in eV, and q_e is the parallel heat flux density. It is assumed that the cross-field heat flux-divergence is uniform

within the main-chamber region ($\frac{dq_e}{ds} = Q_{SOL} = \text{constant}$). Constant radiation losses are assumed in

the region below the x-point is assumed ($\frac{dq_e}{ds} = -Q_{rad}$). In this model Q_{SOL} and Q_{rad} (in units

of W/m^3) are used as adjustable parameters to match measured T_e values at the outer midplane and target.

The solver uses a combination of the continuity and momentum equations to solve for n_e and the ion velocity, v_p , on the flux tube:

$$\frac{d}{ds} (n_e v_p) = n_e n_o \langle \sigma v \rangle_{iz} - n_e^2 \langle \sigma v \rangle_{rec} \quad (2)$$

$$\frac{d}{ds} (n_e m v_p^2 + 2n_e T_e) = -m n_o v_p v_{mom} \quad (3)$$

In Eqs. 2 and 3, n_o is the plasma neutral density, ν_{mom} is the frequency of momentum transfer between the plasma ions and neutrals, ‘iz’ denotes ionization and ‘rec’ denotes recombination. The information on n_o is iteratively estimated by the EIRENE neutral transport code using the plasmas from DIVIMP. An *ad hoc* model is used for detached regions to estimate the detachment front location as well as the n_e and T_e profile [4]. Fig.2 shows the parallel flow obtained from the current model and measurements of plasma flow [7] (thicker line) in the first flux tube outside the separatrix. The measured flow is larger than the model, typically by a factor of ~ 3 at the inboard. This difference could be due to the fact that the current model does not include transport-driven parallel flows and the Pfirsch-Schluter current, which have been inferred from the experiment [7]. The general flow pattern, however, is obtained in the model: the parallel plasma flow is directed from the outboard to the inboard and becomes larger as the inboard is approached (‘reference’ case of Fig.2). Due to the lack of model and measurements, the plasma profile in the private flux region is provided by ‘empirical reconstructive’ OEDGE modeling where the private flux zone plasma parameters are inferred by matching D_α and D_γ signals in the divertor and Stark broadening measurements [8].

3. Asymmetry of Screening of Inboard vs. Outboard for Non-recycling Model

In our DIVIMP modeling of the penetration factor, we utilize carbon impurities which do not recycle from surfaces. The modeling has qualitatively reproduced the asymmetry of impurity screening of inboard vs. outboard (see Fig.3, ‘reference case’). We define the code penetration factor (PF) as

$$PF_{I,K}(\%) = \frac{\# \text{ of ions entering core from a grid element I,K}}{\# \text{ of neutrals injected into a grid element I,K}} \times 100(\%) \quad (4).$$

A different definition of PF was employed in [1]. However, the focus here is on the *patterns* and *trends* which are expected to be similar, based on either definition. The poloidal variation of PF for the reference flow case and low density is shown in Fig.3 (circle symbols). To better approximate experiment, a regional penetration factor is calculated by averaging over a range in source locations indicated in Fig. 3. The resultant averaged PF (%) is 3.6 for inboard, 11 for outboard, and 0.7 for divertor sources. The variation in the ratio of outboard to inboard PF is qualitatively consistent with experiment [1].

We have examined the sensitivity of PF to the plasma flow and the impurity injection energy. To estimate the effect of flow on screening, the plasma flow has been increased primarily at the inboard region to match, across the SOL, the measured flow values. This results in the reduction of the inboard region PF by a factor of 3 while the PF for the outboard and divertor regions remain relatively unchanged (Fig.3). Certainly, the inclusion of a better match to the measured flow [7] better matches C-Mod PF_{NR} results.

To estimate the strength of the dependence of PF on injection energy, the reference injection energy (0.03 eV) was increased to 0.5 eV at the outboard edge. Such an increase of the energy allows the neutrals to penetrate deeper into the SOL ionizing closer to the separatrix. As a result the local PF is increased almost by a factor of 5 as shown in Fig.3. There is a potential for such a poloidal variation in injection energy, e.g. caused by sheath rectification near an ICRF antenna [9], or locally enhanced heat transport at the outboard.

To complement the analysis of PF based on non-recycling impurities we have also generated a PF profile by allowing impurities to recycle from surfaces. Forty ‘argon’ impurity neutrals are launched from the outboard edge with each allowed 2,000 recyclings (total of 80,000 recyclings) spread over the various locations (shown in Fig.1). The number of recyclings allows the modeling to reach a steady state and the core impurity level (defined by the total number of

impurity ions crossing separatrix) to be independent of the initial injection location as seen in experiment [2]. The model (**sepxing**) tabulates each inward crossing of the separatrix and which solid surface the particle *last* touched before crossing the separatrix. The PF pattern of Fig.3 is roughly reproduced utilizing recycling impurities in this manner.

We can also use this model to make a comparison with the experimental values for the global recycling penetration factor, PF_R [2]. Table 1 provides the number of Ar ions reaching the core ($\equiv I_{TOT}$) in the three density cases. The number launched is, as mentioned earlier, 80,000, leading to a recycling PF of 3.2%, 2.3% and 4.3% in low, medium and high density cases respectively. Turning on increased flows reduces the recycling PF for all but the detached case and gives values similar to experiment (3 - 0.7%) [2]. The PF drops in going from low to medium density as in experiment, although for the detached case it rises again (not matching experiment).

Further correlation with experiment is seen in the time dependence of the core Ar level and its relation to injection locations. In the recycling model and experiment impurities launched from the outboard (inboard and divertor) initially lead to a core Ar level higher (lower) than steady state (Fig. 3 of [2] and Fig. 6-3 of [4]). As the number of recyclings increases in the model the dependence of core Ar level on initial launch location disappears as seen in the experiment. Ar redistributes poloidally such that less Ar is in the outboard SOL and more is in regions of lower PF. If we calibrate the equilibrium time in the model (which is '500' recyclings) to that in the experiment (that is ~ 20 ms), we obtain a recycling time scale of ~ 40 μ sec/recycling. Thus, each Ar travels a small distance between recyclings, of order 0.1 m. This appears reasonable and gives us more confidence in the model.

4. Relationship of Recycling Sources to the Core Impurity Level

In addition to studying the screening (PF) of impurities, we have explored the relative importance of various recycling sources and how those impurities flow into the core. The **sepxing** counter gives the number of ions that cross the separatrix into the core (I_{TOT}) with the value for the low density case being 2,570. The medium and high density (detached) plasmas have 1,848 and 3,413, respectively. Since **sepxing** also keeps track of which solid surface the particle last recycled from, we can determine the relative importance of each source in setting the core impurity level. We define S_x (e.g. S_{IWL} , S_{OWL} , S_{IT} , and S_{OT}) to be the number of impurity ions entering the core from source location, 'x'. The ratio of S_x to I_{TOT} is summarized in Table 1. The results show that the outboard source S_{OWL} , dominates the core impurity influx ($S_{OWL}/I_{TOT} \sim 70\%$) compared to other source locations for all density cases (and the reference flow case). The effect of increased plasma flow (Table 1, inside parentheses) reduces the relative importance of the inboard recycling source while it increases the relative importance of the target source: Even with an unchanged divertor PF, increased inboard SOL flow sweeps more ions into the divertor, increasing recycling there, thus increasing its importance in determining the core impurity level. This effect is particularly strong for the high density case.

We can also use **sepxing** to determine where impurity ions cross the separatrix into the core. Fig. 4 shows the poloidal variation (by separatrix cell number - see Fig. 1) of the number of impurity ions penetrating into the core across the separatrix. It indicates that more ions are flowing into the core from the outboard side than from the inboard side. The outflux pattern (not shown) roughly mirrors that seen for the influx in that the dominant path for impurities leaving the core is at the inboard side [4]. We define I_{INB} , I_{OBD} , and I_{XP} to be the number of ions entering the core integrated across the separatrix locations (27-41), (42-59), and (60-62) respectively. I_{TOT} and ratio of I_x/I_{TOT} are given in Table 2. The effect of increased flow is again indicated inside

parentheses. By comparison of Tables 1 and 2 it appears that impurities, for each time they cross the separatrix, generally do not travel far poloidally before entering the core. Of course, over many recyclings, they can migrate much farther poloidally.

There are several other implications of Table 2. The impurity inward flux across the separatrix from the inboard side is in excess of the inboard recycling source (Table 1), and the influx through the x-point region is significant for low and high density plasma cases becoming even more important with increased SOL flows. The first observation implies that a small fraction of the ions recycled at the outboard travel to the inboard region and then penetrate into the core from that region, before making contact with another solid surface. Regarding the second observation, the increase in the importance of the divertor source is driven by the increased impurity fluxes there.

5. Discussion

In the cases where impurity penetration through the x-point region is significant (low and high density cases), parallel impurity ion flows in the SOL just outboard of the x-point appear to be the dominant factor. Apparently, the impurity ion flows there are directed upstream (both the frictional and ion temperature gradient forces push the ions away from the target). For the medium density case, impurity ion flows are instead toward the outer target in the x-point region. We note that there is always an impurity flow near the separatrix in the outboard SOL towards the divertor. Thus when there is a simultaneous flow of ions out of the divertor the two flows ‘meet’, stagnating near the x-point, and the ions diffuse radially, some crossing the separatrix.

It is clear that improvements in the plasma model are needed. When a consistent profile of n_e and T_e are implemented the inboard SOL flow does not match experiment. Forcing a match of the flows to experimental values [7] (ad hoc and not self-consistent) allows a better PF match with

experiment. Similarly the detail of the T_i profile is unknown in the divertor and x-point regions and its parallel gradient greatly affects the importance of the divertor impurity sources on core impurity levels. Nevertheless the model has been, and was used, to generally match the experimental measurements for recycling and non-recycling PF, to characterize the impurity flow pattern, and to determine the important factors governing impurity penetration and flow. Since the plasma characteristics outside the divertor are better known it is our opinion that the transport of impurities generated outside the divertor are better modeled in this study.

6. Summary

DIVIMP modeling has qualitatively reproduced the general poloidal pattern of the penetration factor observed in experiment for non-recycling impurities. The PFs for impurities launched from the inboard and target regions are lower than from the outboard region. Increasing inboard plasma flows to levels matching experiment leads to better match of PFs from modeling to experiment. The same study was done for recycling impurities and the match of the model global PF to experiment was fairly good both in magnitude and time dependence.

The outboard source generally dominates over the inboard source by a factor of 4~8 in determining the core impurity level for low and medium density plasmas (attached). This is due to a combination of high penetration factor and strong recycling in that region. At the highest density, for the detached case, divertor impurity sources dominate the core impurity levels.

Acknowledgements

This work is supported by US Department of Energy Contract No. DE-FC02-99ER54512.

References

- [1] G. M. McCracken, B. Lipschultz, B. LaBombard et al, Phys. Plasmas **4** (1997) 1681.
- [2] G. McCracken, R.S. Granetz, B. Lipschultz et al, J. Nucl. Mater. **241-243** (1997) 777.
- [3] P.C. Stangeby and J.D. Elder, J. Nucl. Mater. **220-223** (1995) 193.
- [4] T. Chung, Ph.D. Thesis, ‘Study of recycling impurity retention in Alcator C-Mod’, MIT/PSFC report #RR-04-01, DOE-ET-54512-349, 2004.
- [5] IAEA, Data Compendium for Plasma-Surface Interactions, Nucl. Fusion 1984.
- [6] P.C. Stangeby, *The Plasma Boundary of Magnetic Fusion Devices* (Ch.6.) IoP, 2000, Bristol and Philadelphia.
- [7] B. LaBombard, J. Rice, A. Hubbard et al., Nucl. Fusion **44** (2004) 1047.
- [8] S. Lisgo, Ph.D. Thesis, ‘Interpretive modelling of the Alcator C-Mod divertor’, Univ. of Toronto, 2004.
- [9] B. Lipschultz, D. Pappas, B. Labombard, et al., Nucl. Fusion **41** (2000) 585.

Figure Captions

Fig.1 The DIVIMP computational grid with the recycling locations indicated. The circled number indicates the grid index on the separatrix.

Fig.2 Parallel plasma flow in the SOL just outside the separatrix as used in the model (‘reference case’). Measured flow (shown in thicker lines) are generally larger than model.

Fig.3 Poloidal variation of PF for the non-recycling model and medium density case. The effect of increased flows and locally enhanced injection energy are shown

Fig.4 Poloidal variation of the number of ions (counted by the sepxing) crossing the separatrix is plotted. Separatrix grid element index is shown in Fig. 1.

Table Captions

Table 1. The global PF is tabulated along with the relative importance of each recycling source in determining I_{TOT} . The effect of the increased plasma flow is given inside parentheses.

Table 2. The fraction of the impurity inward flux across the separatrix through the different poloidal regions. The effect of increased plasma flow is indicated in parentheses.

Plasma density	PF (%) $\frac{I_{TOT}}{80000}$	I_{TOT}	Relative source importance, S_X / I_{TOT} (%)		
			Inboard $\frac{S_{IWL}}{I_{TOT}}$	Outboard $\frac{S_{OWL}}{I_{TOT}}$	Target $\frac{S_{IT} + S_{OT}}{I_{TOT}}$
Low	3.2 (1.8)	2570 (1438)	12 (3)	68 (58)	20 (39)
Medium	2.3 (1.3)	1848 (1069)	17.8 (6)	76 (70)	6 (24)
High	4.3 (4.5)	3413 (3615)	7.4 (0.8)	70.3 (39)	22.3 (60)

Table 1, Chung et al., Paper #278, 1 column wide

Plasma Density	I_{TOT}	Regional Influx Fraction (%)		
		I_{INB} / I_{TOT}	I_{OBD} / I_{TOT}	I_{XP} / I_{TOT}
Low	2570 (1438)	14 (4.8)	65 (52.7)	21 (42.4)
Medium	1848 (1069)	25 (15)	68.5 (66)	6.5 (24)
High	3413 (3615)	8.8 (6.4)	66 (44.4)	25.2 (49.2)

Table 2, Chung et al., Paper #278, 1 column wide

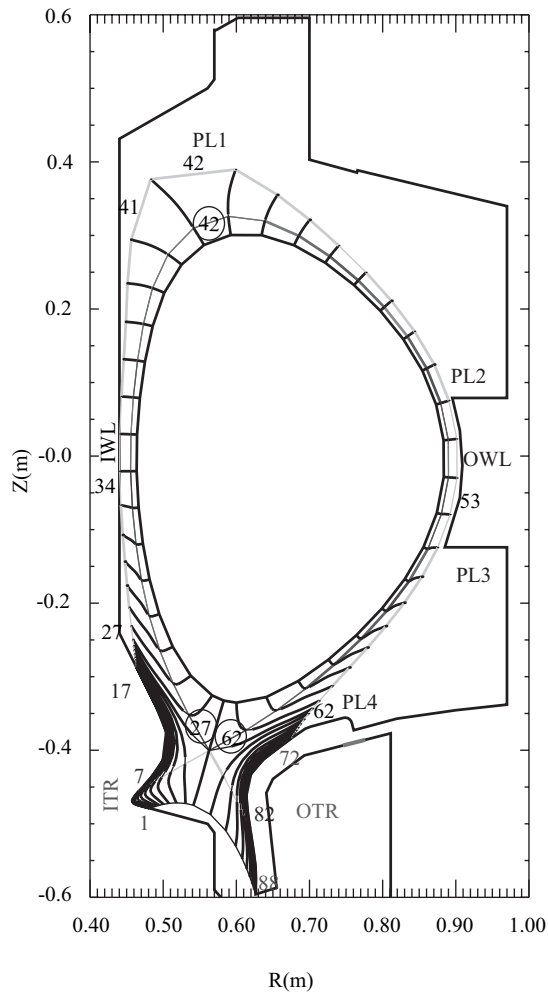


Fig.1, Chung et al., Paper #278, 1 column wide, B/W

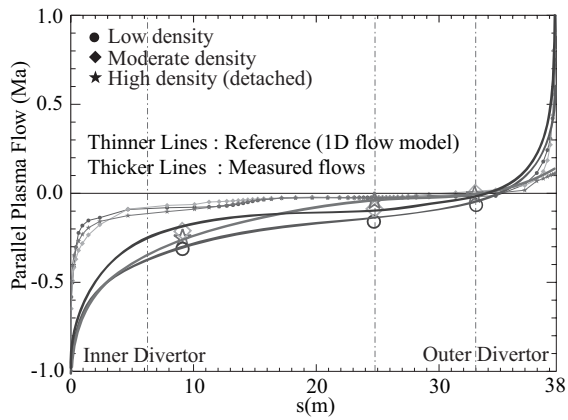


Fig.2, Chung et al., Paper #278, 1 column wide, B/W

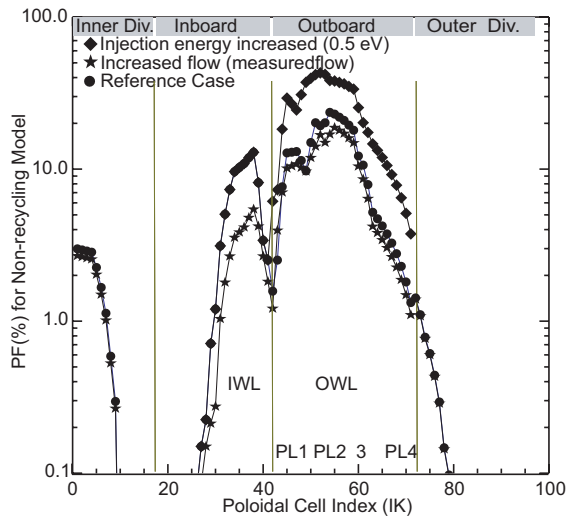


Fig.3, Chung et al., Paper #278, 1 column wide, B/W

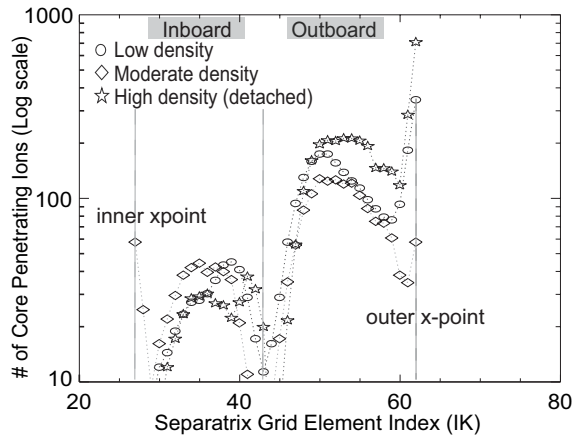


Fig. 4, Chung et al., Paper #278, 1 column wide, B/W